

Probing charge redistribution at the interface of self-assembled *cyclo-P₅* pentamers on Ag(111)

Received: 10 January 2024

Accepted: 23 July 2024

Published online: 02 August 2024

Check for updates

Outhmane Chahib¹, Yuling Yin^{2,3}, Jung-Ching Liu¹, Chao Li¹, Thilo Glatzel¹, Feng Ding^{2,3}, Qinghong Yuan⁴, Ernst Meyer¹✉ & Rémy Pawlak¹✉

Phosphorus pentamers (*cyclo-P₅*) are unstable in nature but can be synthesized at the Ag(111) surface. Unlike monolayer black phosphorous, little is known about their electronic properties when in contact with metal electrodes, although this is crucial for future applications. Here, we characterize the atomic structure of *cyclo-P₅* assembled on Ag(111) using atomic force microscopy with functionalized tips and density functional theory. Combining force and tunneling spectroscopy, we find that a strong charge transfer induces an inward dipole moment at the *cyclo-P₅/Ag* interface as well as the formation of an interface state. We probe the image potential states by field-effect resonant tunneling and quantify the increase of the local change of work function of 0.46 eV at the *cyclo-P₅* assembly. Our experimental approach suggest that the *cyclo-P₅/Ag* interface has the characteristic ingredients of a p-type semiconductor-metal Schottky junction with potential applications in field-effect transistors, diodes, or solar cells.

Elemental phosphorus (P) is not only ubiquitous in human life, it is also one of the most fascinating areas of chemistry as it can exist in a large diversity of allotropes^{1–3}, in various cluster configurations^{4,5}, or in organic compounds⁶. The phosphorous polymorphism is even multiplied on the atomic scale when using a surface to constrain the reaction in two dimensions (2D). As in the field of on-surface chemistry producing complex nanographene structures in ultra-high vacuum (UHV)^{7,8}, surface-assisted phosphorus reactions on metals have synthesized blue phosphorus⁹, P chains¹⁰, or even planar *cyclo-P₅* rings^{11,12}. Since then, phosphorus allotropes have emerged as a promising one-atom thick 2D material beyond graphene, due to its moderate direct band gap (0.3 to 2.0 eV)¹³ suitable for nanoelectronics and nanophotonics applications^{14,15}. However, allotropic configurations, their atomic buckling, defects, or potential alloy formation can be detrimental to the semiconducting character. In addition, the interaction of 2D materials with delocalized electrons of metal, as well as the dynamical charge transfer

between the two media, are key factors in fostering gate-tunable functionalities such as superconductivity^{16,17}. Experimental study of these aspects at the fundamental level is therefore essential for future quantum applications where metallic electrical contacts are required¹⁸.

Low-temperature scanning probe microscopy is an incontrovertible tool for assessing atomic structures in contact with metals and characterizing their electronic properties with high spectral resolution in UHV. Atomic force microscopy (AFM) with functionalized tips^{19,20} has demonstrated real-space imaging with improved lateral and vertical resolution of aromatic molecules and cyclo-carbons²¹. Recently, AFM imaging and spectroscopy have also tackled mono-elemental 2D materials demonstrating a precise quantification of the atomic buckling in these structures^{22,23}. Not only restricted to structural characterization, charge distributions, and work function changes are also accessible at the nanometer scale using Kelvin probe force microscopy (KPFM)^{24–27}. In addition,

¹Department of Physics, University of Basel, Basel, Switzerland. ²Institute of Technology for Carbon Neutrality, Shenzhen Institute of Advanced Technology, Shenzhen, People's Republic of China. ³Faculty of Materials Science and Energy Engineering, Shenzhen University of Advanced Technology, Shenzhen, People's Republic of China. ⁴State Key Laboratory of Precision Spectroscopy, School of Physics and Electronic Science, East China Normal University, Shanghai, People's Republic of China. ✉e-mail: ernst.meyer@unibas.ch; remy.pawlak@unibas.ch

the investigation of the local density of states (LDOS) of 2D materials near the Fermi level is readily achieved by means of STM and scanning tunneling spectroscopy (STS). Tunneling spectroscopy can also probe the image potential states (IPS) of 2D synthetic materials, as demonstrated in the case of graphene²⁸, germanene²⁹, or borophene^{30,31}. Quantifying these Stark-shifted unoccupied states lying below the vacuum level gives not only access to the fundamental physical processes involved in charge carrier dynamics but also to quantify local modulations of the work function at the interface between 2D materials and metals.

By applying this methodology, we determine here the structure of phosphorus chains and self-assembled *cyclo*-P₅ pentamers on Ag(111) using low-temperature (4.5 K) AFM imaging with CO-terminated tips. KPFM spectroscopic measurements indicate the formation of an inwards dipole moment at the P₅/Ag interface, which results from the charge transfer from the Ag substrate to the network, as confirmed by DFT calculations. This charge transfer leads to a complex charge redistribution and the formation of an interfacial hybridized state (IS). Through FERT and STS spectroscopy, we determined the energy position of the IS and the series of IPS at the *cyclo*-P₅ assembly as compared to pristine Ag, confirming an increase of the local work function of ≈ 0.46 eV. We found that the P₅/Ag system behaves as a prototypical p-type semiconductor-metal junction with a Schottky barrier built at the interface, opening prospects for its use in field-effect transistors, diodes, or solar cells. Given the general interest in tailoring the physical characteristics of monoelemental 2D materials contacted to a metal, we think that our experimental approach might serve as a powerful asset for deciphering the energy level alignment of future devices involving electric contacts.

Results

Atomic-scale imaging of the *cyclo*-P₅

Phosphorus atoms were sublimed in UHV onto the Ag(111) substrate, kept at about 423 K (see “Methods”). Figure 1a shows an STM overview image of the resulting structures for a relative coverage of less than 0.3 monolayer (ML). Similar to refs. 10,11, extended 1D chains aligned along the $[\bar{1}\bar{1}0]$ directions of Ag(111) (marked 1) in Fig. 1a) coexist with domains of P₅ molecules (2). The inset of Fig. 1a further shows a STM image of the double and triple chains, which depends on the P deposition rate¹¹.

To precisely determine their atomic configurations, we employed AFM imaging with CO-terminated tips (see “Methods”, Fig. 1c, d)⁹. A common AFM contrast is observed for all configurations assigned to an armchair structure of the chain, which resembles that of hydrocarbon chains³². In each configuration, the chain has always an apparent width by AFM of 6.0 Å with a minimum distance between them of 0.25 Å. Thus, double and triple chains have apparent widths of 14.5 and 23 Å, respectively. The relaxed structure of the triple chain configuration calculated by DFT is shown in Fig. 1e. Phosphorus atoms colored in orange sit on bridge sites of the Ag lattice (gray) and are aligned along one $[\bar{1}\bar{1}0]$ direction in accordance with the experimental data. Based on the DFT coordinates, we simulated the AFM image (see “Methods”, Fig. 1f). The excellent agreement with the experimental image of Fig. 1d confirms the armchair structure of the P chains on Ag(111), similar to ref. 10.

Increasing the P coverage to about 0.4 ML while keeping the substrate at 423 K leads to the formation of large islands of *cyclo*-P₅ pentamers relative to the chains (Fig. 2a)¹². In Fig. 2b, the close-up STM image reveals the structure of the self-assembled domains consisting of a hexagonal lattice with parameters $a_1 = b_1 = 7.6$ Å. Each bright

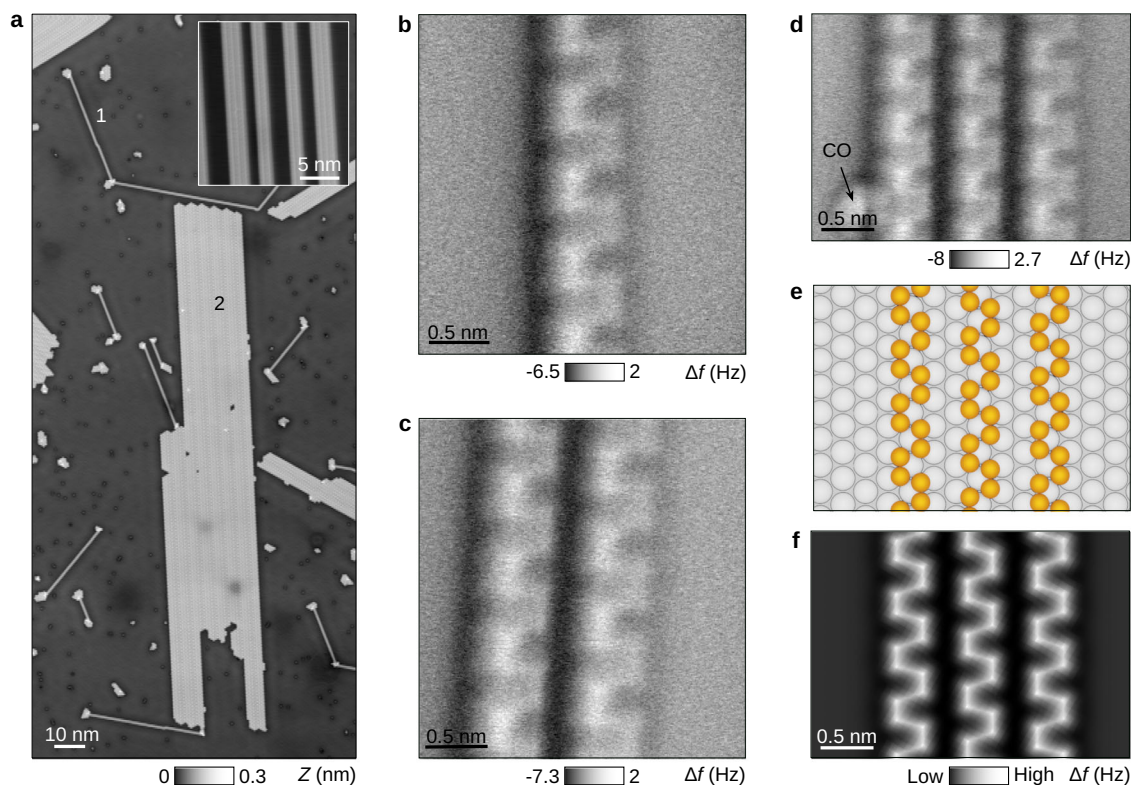


Fig. 1 | Atomic structure of phosphorus chains on Ag(111). **a** STM topographic image after sublimation of phosphorus atoms on Ag(111) leading to P chains (1) and *cyclo*-P₅ domains (2), ($I_t = 1$ pA, $V_s = 0.15$ mV). The inset shows an STM image of the single, double, and triple chains, respectively. **b–d** Series of AFM images with CO-terminated tip revealing the armchair structure of single, double, and triple P

chains, ($f_0 = 26$ kHz, $A = 50$ pm). Scale bars are 0.5 nm. **e** Atomic configurations of the triple armchair chains obtained by DFT calculations. Phosphorus and silver atoms are shown in orange and gray, respectively. **f** Corresponding AFM simulation using the DFT coordinates.

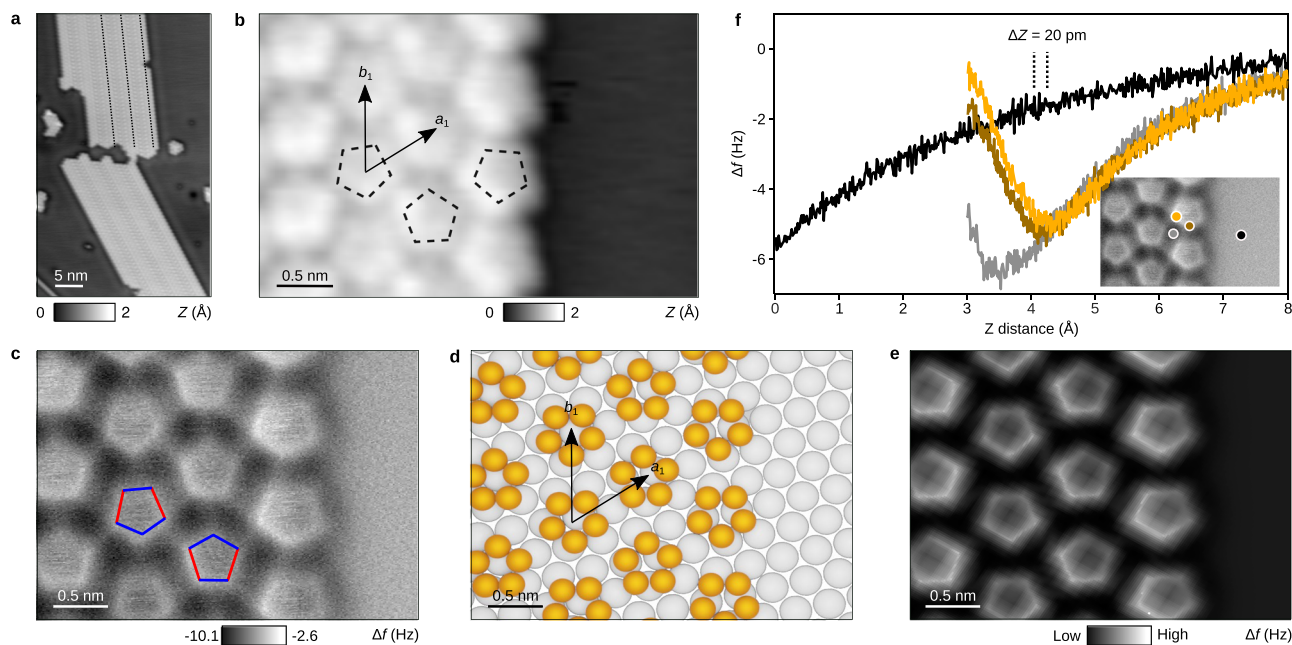


Fig. 2 | Atomic structure of the self-assembled *cyclo-P₅* molecules. **a** STM image of the self-assembled pentamers on Ag(111), ($I_t = 1$ pA, $V_s = 0.15$ mV). Islands systematically show a superlattice of bright lines rotated by 19° with respect to the $[\bar{1}\bar{1}0]$ directions of Ag(111) (dotted lines). **b** Close-up STM topography showing the P_5 pentamers depicted by dashed lines. **c** Corresponding AFM image revealing the P_5 chemical structure, ($f_0 = 26$ kHz, $A = 50$ pm). Each *cyclo-P₅* ring is composed of three short bonds (blue) and two longer ones (red), respectively. **d** Atomic configurations

of the pentamer assembly on Ag(111) obtained by DFT. Phosphorus and silver atoms are shown in orange and gray, respectively. **e** Corresponding AFM simulation using the DFT coordinates. **f** Site-dependent $\Delta f(Z)$ spectroscopic curves acquired at two neighboring P atoms of a P_5 molecule (orange and brown), between two P_5 molecules (gray) and on Ag(111) (black), respectively. The local minima of the $\Delta f(Z)$ curves indicate the relative height of the phosphorus atoms.

protrusion corresponds to one *cyclo-P₅* molecule as schematized by the black dashed pentagons. Domains of *cyclo-P₅* rings exhibit a superstructure characterized by stripes separated by ≈ 4.56 nm (i.e., six P_5 rows), as shown by black dotted lines in Fig. 2a. These lines are rotated by 19° as compared to the $[\bar{1}\bar{1}0]$ directions of the Ag(111) substrate, which agrees with previous experimental works¹¹ as well as the relaxed structure obtained by DFT calculations of Fig. 2d. We thus confirm that the *cyclo-P₅* assembly adopts a $(\sqrt{7} \times 6\sqrt{7})R19^\circ$ unit cell with respect to the Ag(111) surface lattice as previously reported by Zhang et al.¹¹

A deeper insight into the chemical structure of the *cyclo-P₅* molecules is provided by the AFM image in Fig. 2c. We also simulated the AFM image based on DFT coordinates, allowing us to confirm the exact position and structure of the P_5 molecules in their self-assembly in registry with the Ag(111). The P-P bond length within the *cyclo-P₅* pentamer extracted by AFM varies from 2.5 to 2.7 Å, which is always larger by about 8% than that of DFT calculations for the pentamer on Ag(111) (Fig. 2d and Supplementary Fig. 1) or in the gas phase (2.185 Å)³³. It is well-established that this overestimation of apparent bond lengths is induced by the tilting of the CO molecule attached to the AFM tip upon scanning, as shown for planar polyaromatic hydrocarbons or P_3N_3 molecules^{34,35}. Moreover, each *cyclo-P₅* ring is composed of three short apparent bonds (2.5 Å, blue bonds in Fig. 2c) and two longer ones (2.7 Å, red bonds). This particular bond order, also confirmed in the relaxed structure calculated by DFT (Fig. 2d), is likely induced by the small buckling of the structure when adsorbed on Ag(111).

To accurately quantify the atomic corrugation within the *cyclo-P₅* structure, we acquired a series of site-dependent $\Delta f(Z)$ spectroscopic curves (Fig. 2f) at the locations marked in the inset AFM image. The black and gray curves were obtained on Ag and between two pentamers, respectively. On top of neighboring atoms of a *cyclo-P₅* (orange and brown curves), spectra exhibit a characteristic dip arising from the interaction between the front-end oxygen atom of the CO-terminated

tip with the phosphorus atom. The dashed vertical lines indicate the Z position of their bottoms and are the signature of the relative atomic Z height²³. The difference ΔZ of ≈ 20 –30 pm thus represents the intrinsic atomic corrugation within the *cyclo-P₅* pentagonal structure⁵, which is comparable with atomic corrugations in graphene³⁶ or planar molecules³⁷. Thus, this confirms the planarity of the *cyclo-P₅* structure⁵, as reflected in the constant-height AFM image of Fig. 2e.

Charge distribution at the P_5 /Ag interface

Through DFT calculations, it has been determined that the cyclic P_5 pentamer exhibits a higher binding energy on the Ag(111) surface, amounting to -0.90 eV per atom (Supplementary Fig. 2). This larger energy value is primarily facilitated through a charge transfer mechanism, promoting the stability of the cyclic P_5 structure. To provide insights into the charge distribution at the *cyclo-P₅* interface, we performed force versus voltage spectroscopic measurements (see “Methods”). Experimentally, the frequency shift Δf as a function of the sample bias V_s is measured at a constant tip height Z , providing in the $\Delta f(V)$ curve a parabola due to the electric force acting between tip and sample. The voltage V^* at the top of the parabola represents the local contact potential difference (LCPD) between tip and sample, which allows one to image charge distributions and work function changes with nanoscale resolution^{24–27}. Figure 3a shows a $\Delta f(V)$ cross-section acquired across a P_5 domain (see STM inset of Fig. 3a). Single $\Delta f(V)$ point-spectra on top of the P_5 network (orange) and on Ag(111) (black) are plotted in Fig. 3b, respectively. The dashed lines in Fig. 3a, b refer to the V^* position. The LCPD value systematically shifts towards positive values ($\Delta V^* \approx 0.22$ V) for the pentamer assembly as compared to the pristine Ag substrate. This indicates the accumulation of charges at the P_5 network as compared to the Ag substrate.

To better rationalize this, we calculated the charge redistribution at the *cyclo-P₅*/Ag interface (see “Methods”), whose top and side views of isosurfaces of electron accumulation (blue, $+13 \times 10^{-3} e \text{ \AA}^{-3}$) and depletion (red, $-13 \times 10^{-3} e \text{ \AA}^{-3}$) are displayed in Fig. 3c. An electron

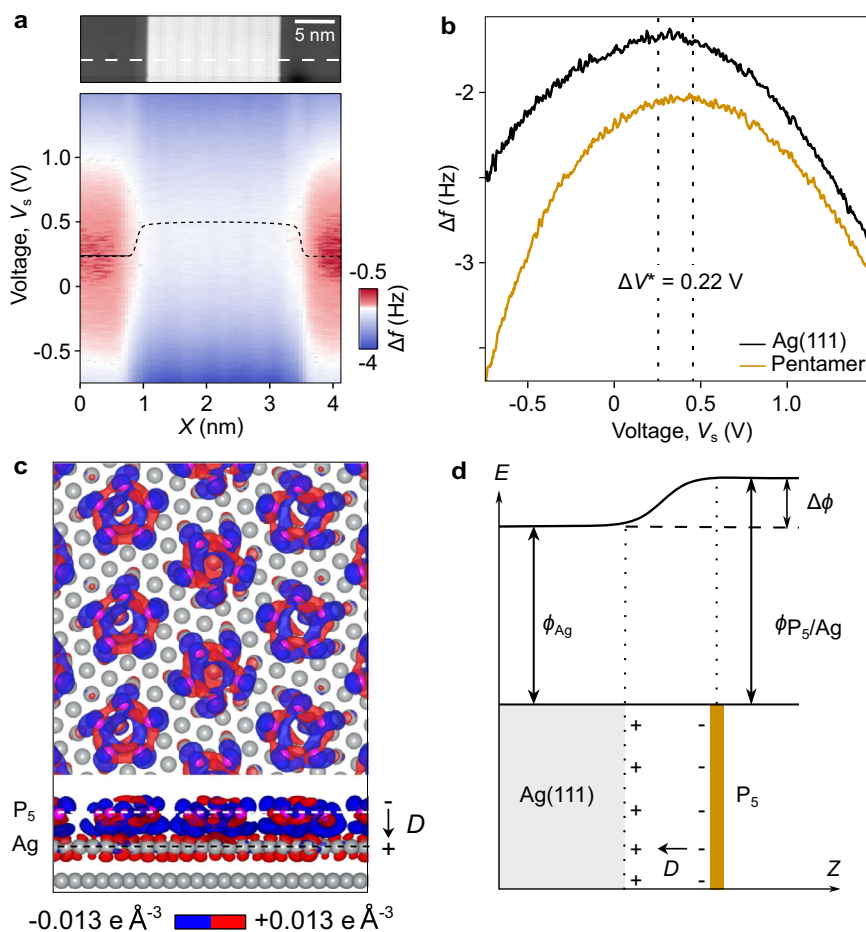


Fig. 3 | Charge redistribution at the *cyclo*-P₅/Ag(111) interface. **a** Frequency shift Δf as a function of sample bias voltage V_s , measured across a pentamer domain shown in the STM image by a dashed line, (parameters: $f_0 = 26$ kHz, $A = 80$ pm). **b** Single $\Delta f(V)$ curves at the pentamer assembly (orange) as compared to the Ag(111) (black). Dashed lines mark the top of the parabola allowing the extract an LCPD shift $\Delta V^* = 0.22$ V. **c** Top and side views of the charge redistribution between

pentamers and Ag(111). Blue (red) areas show electron accumulation (depletion). The white and black dashed lines refer to the position of the P₅ assembly and the last Ag layer, respectively. The isosurface level of the plot is set to $\pm 13 \times 10^{-3} e \text{ \AA}^{-3}$. **d** Schematic illustration of the charge redistribution at the P₅/Ag(111) interface leading to an inward surface dipole (D) moment and a local work function change ($\phi_{P_5/Ag}$). The *cyclo*-P₅ layer is colored orange. ΔV refers to the LCPD change.

transfer from the Ag(111) substrate to the P atoms of pentamers is observed as a negative charge accumulation located at the *cyclo*-P₅ ring (red). In the P₅/Ag gap (marked by white and black dashed lines in the side view in Fig. 3c), charge accumulation/depletion layers emerge below each *cyclo*-P₅ structure, which supports the formation of a hybridized state^{30,31}. We emphasize that such an interface state is not restricted to 2D Xenon on metals since it has been observed for organic/metal systems³⁸.

Between *cyclo*-P₅ rings, we note the absence of in-plane charge redistribution. Considering that the last Ag layer is depleted (red) while each *cyclo*-P₅ has an excess of negative charges (blue), the P₅ assembly can be approximated to a lattice of surface dipole moments of $D = 1.42$ Debye pointing towards the substrate (see arrow in Fig. 3c). The observation of such surface dipole moments is consistent with an increase of the LWF at the P₅/Ag interface, fixed to an arbitrary value $\Delta\phi$ in the diagram of Fig. 3d. While the LWF increase agrees with the LCPD shift to more positive values in force spectroscopy, it is important to note that the LCPD variations are a qualitative indicator of the LWF changes at the atomic scale since it can have a strong distance-dependence on metal substrate^{39,40}. Indeed, the ΔV^* cannot directly account for the difference of work function $\Delta\phi = \phi_{P_5/Ag} - \phi_{Ag}$ shown in Fig. 3d due to the averaging effects of the electrostatic interactions between tip and sample and the uncertainty in the work function of the tip. As will be discussed later, a

quantitative experimental value of LWF (0.46 eV) can be obtained by the analysis of IPS spectra.

Finally, the planar *cyclo*-P₅ structure has, in principle, an unpaired electron leading to an anionic state (i.e., *cyclo*-P₅⁻), which has been identified by nuclear magnetic resonance (NMR) in the gas phase or as a ligand^{41,42}. Upon adsorption on Ag(111), the *cyclo*-P₅⁻ anion can coordinate with the Ag atoms below it, leading to a charge redistribution at the interface and the formation of an interfacial state. This charge transfer modifies the amount of charge of the pentamer away from an integer, as confirmed by the Bader charge analysis showing an accumulation of electrons on P atoms ($-0.115 e$) and an electron depletion ($+0.061 e$) of the depleted Ag layer. We, therefore, conclude that *cyclo*-P₅ molecules do not retain their anionic character on Ag(111). This conclusion is further corroborated by the absence of a Kondo resonance or spin excitations in dI/dV spectra acquired near the Fermi level⁴³.

Interface state and work function of the P₅ assembly

To shed more light on the electronic properties at the P₅/Ag interface, we next performed differential conductance measurements (dI/dV) across a P₅ domain (see “Methods”). Figure 4a shows the typical dI/dV point-spectra spectra of the network (orange) as compared to Ag(111) (black). We marked with dashed lines the valence band edge maximum (VBE) at -0.5 eV and the conduction band edge minimum (CBE) at 0.3 eV, providing a gap E_g of the P₅

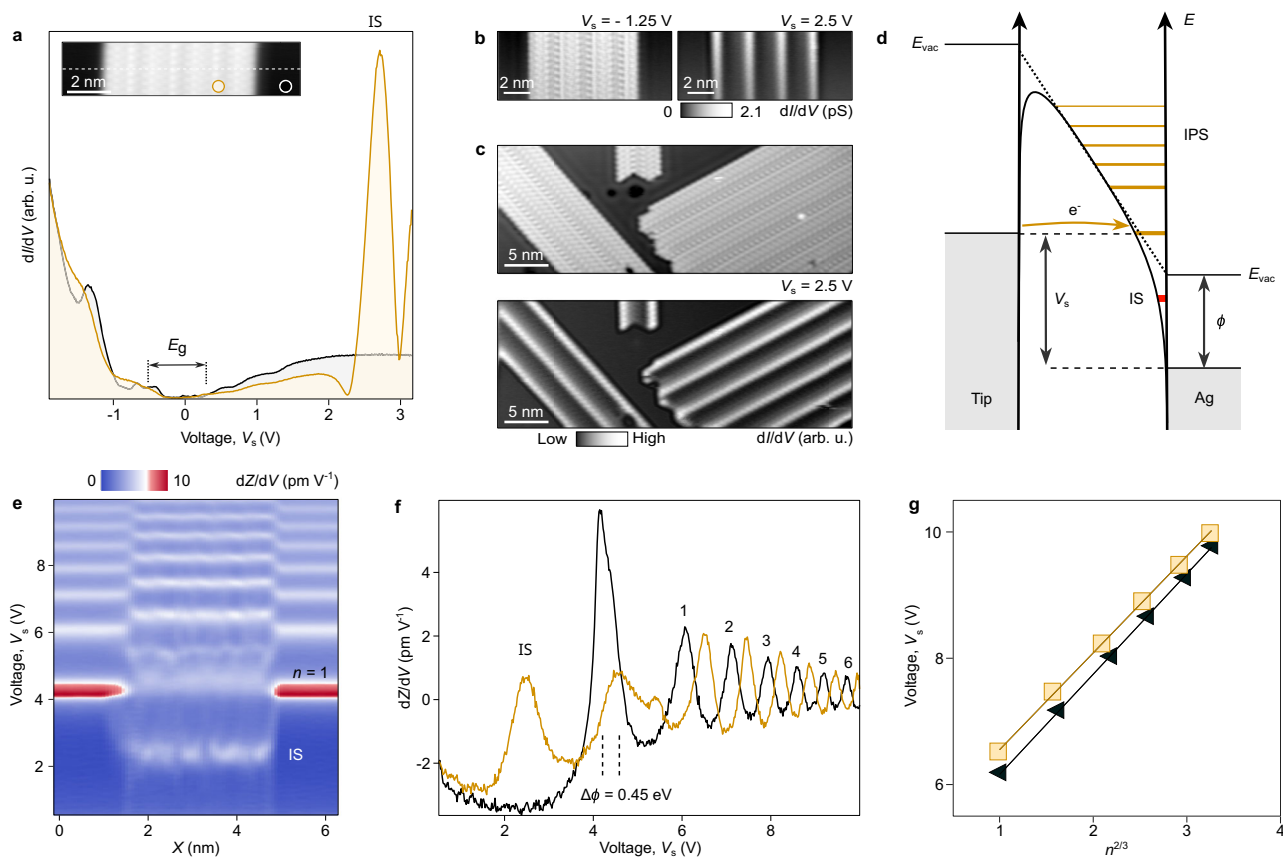


Fig. 4 | Tunneling spectroscopy of the P₅/Ag interface. **a** dI/dV point-spectra acquired above the P₅ assembly (orange) and on Ag(111) (black), whose locations are shown in the STM inset. (parameters: $I_t = 1$ pA, $V_s = 500$ mV, $A_{\text{mod}} = 10$ mV, $f = 511$ Hz). **b** dI/dV maps at $V_s = -1.25$ and 2.5 V, respectively. **c** STM topographic image of three P₅ domains and the corresponding dI/dV maps of the IS modulation.

d Scheme of the band alignment and the formation of Stark-shifted IPS (orange lines). **e** FERT cross-section acquired across the P₅ assembly along the dashed line in (a), (Set-points: $I_t = 1$ pA, $V_s = 500$ mV, $A_{\text{mod}} = 35$ mV, $f = 511$ Hz). **f** Single FERT spectra of the P₅ assembly and the Ag(111) substrate, showing the series of n^{th} IPS. **g** Extracted IPS peak voltages as a function of $n^{2/3}$.

assembly to about 0.8 eV. The spectra also show a strong resonance at 2.5 V, which we attribute to tunneling into an interface state (IS). dI/dV maps (Fig. 4b) further reveal the density of states at the valence band at $V_s = -0.5$ V. This atomic feature evolves to a stripe pattern at $V_s = +2.5$ V (Fig. 4c, bottom), revealing the spatial modulation of the IS (Fig. 4a) similar to the superstructure shown in STM topographic image of Fig. 2a.

To quantify the local change of work function (LWF), we acquired field-effect resonant tunneling (FERT) spectra in order to probe IPS between the *cyclo*-P₅ assembly and silver. Experimentally, FERT spectra (also called dZ/dV spectroscopy) are obtained by sweeping the sample voltage V_s while keeping constant the tunneling current with the STM feedback loop. When the voltage exceeds the local work function, resonant tunneling through the tip-sample junction occurs from the tip into the image potential states, giving rise to a series of peaks in the FERT spectra. From a quasi-classical approximation (Fig. 4d), tunneling resonances occur when the Fermi level of the tip aligns with the Stark-shifted IPS states, see Eq. (1).

$$eV_n = \phi + \left(\frac{3n\pi\hbar eE}{\sqrt{2m}} \right)^{2/3} \quad (1)$$

where V_n is the sample voltage for the n^{th} IPS, ϕ is the work function of the sample, m is the free electron mass, and E is the electric field.

Interestingly, the comparison of FERT spectra between tip positions enables us to distinguish interfacial charge transfer and quantify the local change of work function at the nanometer scale^{28–31}.

Figure 4e, f shows the series of IPS states obtained above the *cyclo*-P₅ self-assembly as compared to Ag(111), respectively. The resonance at $V_s = 2.2$ eV of the orange spectrum of Fig. 4f, which is absent for the Ag one (black), corresponds to the IS. The peaks noted $n = 1$ to 6 of the black spectra are the IPS states of the pristine Ag substrate. On the P₅ assembly, IPS states are clearly shifted to higher voltage when ramping up the electric field (i.e., V_s), which is the signature of the increase of LWF^{30,31}.

A quantitative estimation of the LWF can be obtained from Eq. (1). In Fig. 4g, we plot the voltage position V_n of the IPS states as a function of $n^{2/3}$ for both the *cyclo*-P₅ network (orange squares) and the Ag(111) substrate (black triangles). By fitting the linear progression of each dataset, we extract the LWF value corresponding to the y-intercepts to $\phi_{\text{Ag}} = 4.49$ eV and $\phi_{\text{P}_5} = 4.95$ eV, respectively. Considering that our experimental estimate of ϕ_{Ag} is in agreement with that obtained by ultraviolet photoelectron spectroscopy (UPS)⁴⁴, we quantify the increase of LWF of $\Delta\phi = 0.46$ eV induced by the *cyclo*-P₅ assembly adsorbed on Ag(111). Altogether, the observation of the IS and the shift of IPS resonances in tunneling spectroscopy point to a charge transfer from the Ag substrate to the *cyclo*-P₅ network, leading to the creation of inwards electric dipoles at the interface.

Discussion

In summary, we synthesized phosphorus chains and *cyclo*-P₅ pentamers by depositing phosphorus atoms on atomically flat Ag(111) in an ultra-high vacuum. Using low-temperature AFM with CO-terminated tips, armchair P chains, and *cyclo*-P₅ rings are resolved with atomic precision. DFT calculations support a substantial charge transfer from the Ag substrate to P₅ pentamers, which results in a complex charge redistribution at the P₅/Ag interface. This further leads to the emergence of an interface state as observed by dI/dV spectroscopy. Using force-voltage spectroscopic measurements, we infer the local increase of work function at the P₅ network in comparison to the bare metal substrate and determine the direction of the induced surface dipole moments. We corroborated these measurements with FERT spectroscopy to quantify the LWF increase of 0.46 eV at the P₅/Ag interface. Based on our experimental estimates, we summarize in Supplementary Fig. 3 the energy level alignment at the *cyclo*-P₅/Ag interface. Considering that the Ag metal is depleted while the P₅ assembly is negatively charged, we conclude that the P₅/Ag system behaves as a prototypical p-type semiconductor-metal junction with a Schottky barrier built at the interface. It further shows that this system could have potential applications in field-effect transistors, diodes, or solar cells. Finally, by exploring the fundamental characteristics of the prototypical *cyclo*-P₅/metal interface, our methodology (applicable to other emerging 2D materials and related quantum materials) not only showcases the importance of scanning probe microscopy as a powerful technique to study structural and electronic properties at the atomic scale but also provides insights for improved performances of phosphorus-based devices.

Methods

Sample preparation

The Ag(111) substrate purchased from Mateck GmbH was sputtered by Ar⁺ ions and annealed at 770 K to eliminate any surface contaminations. Phosphorus atoms were sublimed by heating up a black phosphorus crystal contained in a Knudsen cell in an ultra-high vacuum (UHV). The P flux was estimated using a quartz microbalance. To obtain the phosphorus chains and P₅ domains, we annealed the Ag(111) substrate during deposition at temperatures described in ref. 9.

AFM experiments

AFM measurements were performed with commercially available tuning-fork sensors in the qPlus configuration⁴⁵ equipped with a tungsten tip ($f_0 = 26$ kHz, $Q = 10,000$ – $25,000$, nominal spring constant $k = 1800$ N m⁻¹, oscillation amplitude $A \approx 50$ pm). Constant-height AFM images were obtained using tips terminated with a single CO in the non-contact frequency-modulated AFM (FMAFM) mode at zero voltage^{19,46}. CO molecules were adsorbed on the sample maintained at below 20 K. Before its functionalization, the apex was sharpened by gentle indentations into the Ag surface. A single CO molecule was carefully attached to the tip following the procedure of ref. 47. Simulations of the AFM images based on the DFT coordinates were carried out using the probe-particle model⁴⁸. Site-dependent $\Delta f(Z)$ spectroscopic measurements to determine the atomic buckling of phosphorus pentamers were obtained with CO-terminated tips. The $\Delta f(V)$ cross-section of 1×85 pixels was acquired with Ag-coated metallic tips (tunneling setpoints: $I_t = 1$ pA, $V_s = 800$ mV, $Z_{\text{offset}} = +80$ pm).

DFT calculations

All DFT calculations were carried out in the Vienna ab initio simulation package (VASP)⁴⁹ with the projector augmented wave (PAW) method. The generalized gradient approximation (GGA) in the framework of Perdew-Burke-Ernzerhof (PBE)⁵⁰ was chosen with the plane-wave cut-off energy set at 400 eV for all calculations. The DFT-D3⁵¹ method of Grimme was employed to describe the van der Waals (vdW) interactions. The geometries of the structures were relaxed until the force on

each atom was less than 0.02 eV Å⁻¹, and the energy convergence criterion of 1×10^{-4} eV was met. The Brillouin zone was sampled using Gamma k-mesh with a separation criterion of 0.03. Metal slabs with 3 atomic layers were adopted as the substrate, and the bottom layer was fixed to simulate the bulk. The vacuum spacing between neighboring images was set at least 15 Å along the non-periodic directions to avoid a periodic interaction.

Data availability

The data that support the findings of this study are available from Zenodo⁵² and from the corresponding authors upon request.

References

1. Liu, H., Du, Y., Deng, Y. & Ye, P. D. Semiconducting black phosphorus: synthesis, transport properties and electronic applications. *Chem. Soc. Rev.* **44**, 2732–2743 (2015).
2. Carvalho, A. et al. Phosphorene: from theory to applications. *Nat. Rev. Mater.* **1**, 1–16 (2016).
3. Batmunkh, M., Bat-Erdene, M. & Shapter, J. G. Phosphorene and phosphorene-based materials - prospects for future applications. *Adv. Mater.* **28**, 8586–8617 (2016).
4. Jones, R. O. & Hohl, D. Structure of phosphorus clusters using simulated annealing - P2 to P8. *J. Chem. Phys.* **92**, 6710–6721 (1990).
5. Chen, M. D., Huang, R. B., Zheng, L. S., Zhang, Q. E. & Au, C. T. A theoretical study for the isomers of neutral, cationic and anionic phosphorus clusters P5, P7, P9. *Chem. Phys. Lett.* **325**, 22–28 (2000).
6. Giusti, L. et al. Coordination chemistry of elemental phosphorus. *Coord. Chem. Rev.* **441**, 213927 (2021).
7. Cai, J. et al. Atomically precise bottom-up fabrication of graphene nanoribbons. *Nature* **466**, 470–473 (2010).
8. Clair, S. & de Oteyza, D. G. Controlling a chemical coupling reaction on a surface: Tools and strategies for on-surface synthesis. *Chem. Rev.* **119**, 4717–4776 (2019).
9. Zhang, J. L. et al. Epitaxial growth of single layer blue phosphorus: a new phase of two-dimensional phosphorus. *Nano Lett.* **16**, 4903–4908 (2016).
10. Zhang, W. et al. Flat epitaxial quasi-1D phosphorene chains. *Nat. Commun.* **12**, 5160 (2021).
11. Zhang, W. et al. Phosphorus pentamers: floating nanoflowers form a 2D network. *Adv. Funct. Mater.* **30**, 2004531 (2020).
12. Yin, Y., Gladkikh, V., Yuan, Q. & Ding, F. Phosphorus chains and pentamers: The precursors of blue phosphorene on the Ag(111) substrate. *Chem. Mater.* **34**, 8230–8236 (2022).
13. Li, L. et al. Direct observation of the layer-dependent electronic structure in phosphorene. *Nat. Nanotechnol.* **12**, 21–25 (2017).
14. Liu, H. et al. Phosphorene: an unexplored 2D semiconductor with a high hole mobility. *ACS Nano* **8**, 4033–4041 (2014).
15. Wang, X. et al. Highly anisotropic and robust excitons in monolayer black phosphorus. *Nat. Nanotechnol.* **10**, 517–521 (2015).
16. Shao, D. F., Lu, W. J., Lv, H. Y. & Sun, Y. P. Electron-doped phosphorene: A potential monolayer superconductor. *Europhys. Lett.* **108**, 67004 (2014).
17. Zhang, R., Waters, J., Geim, A. K. & Grigorieva, I. V. Intercalant-independent transition temperature in superconducting black phosphorus. *Nat. Commun.* **8**, 15036 (2017).
18. Li, Y., Yang, S. & Li, J. Modulation of the electronic properties of ultrathin black phosphorus by strain and electrical field. *J. Phys. Chem. C* **118**, 23970–23976 (2014).
19. Gross, L., Mohn, F., Moll, N., Liljeroth, P. & Meyer, G. The chemical structure of a molecule resolved by atomic force microscopy. *Science* **325**, 1110–1114 (2009).
20. Mönig, H. et al. Quantitative assessment of intermolecular interactions by atomic force microscopy imaging using copper oxide tips. *Nat. Nanotechnol.* **13**, 371–375 (2018).

21. Kaiser, K. et al. An sp-hybridized molecular carbon allotrope, cyclo[18]carbon. *Science* **365**, 1299–1301 (2019).
22. Liu, X. et al. Geometric imaging of borophene polymorphs with functionalized probes. *Nat. Commun.* **10**, 1642 (2019).
23. Pawlak, R. et al. Quantitative determination of atomic buckling of silicene by atomic force microscopy. *Proc. Natl. Acad. Sci. USA* **117**, 228–237 (2020).
24. Mohn, F., Gross, L., Moll, N. & Meyer, G. Imaging the charge distribution within a single molecule. *Nat. Nanotechnol.* **7**, 227–231 (2012).
25. Schuler, B. et al. Contrast formation in Kelvin probe force microscopy of single π -conjugated molecules. *Nano Lett.* **14**, 3342–3346 (2014).
26. Meier, T. et al. Donor-acceptor properties of a single-molecule altered by on-surface complex formation. *ACS Nano* **11**, 8413–8420 (2017).
27. Pawlak, R. et al. Hydroxyl-induced partial charge states of single porphyrins on titania rutile. *J. Phys. Chem. C* **121**, 3607–3614 (2017).
28. Borca, B. et al. Potential energy landscape for hot electrons in periodically nanostructured graphene. *Phys. Rev. Lett.* **105**, 036804 (2010).
29. Borca, B. et al. Image potential states of germanene. *2D Materials* **7**, 035021 (2020).
30. Liu, X., Wang, L., Yakobson, B. I. & Hersam, M. C. Nanoscale probing of image-potential states and electron transfer doping in borophene polymorphs. *Nano Lett.* **21**, 1169–1174 (2021).
31. Liu, X. et al. Borophene synthesis beyond the single-atomic-layer limit. *Nat. Mater.* **21**, 35–40 (2022).
32. Giovanelli, L. et al. On-surface synthesis of unsaturated hydrocarbon chains through C-S activation. *Chem. Eur. J.* **28**, e202200809 (2022).
33. Jin, Q., Jin, B., Xu, W. G. & Zhu, W. Aromaticity of planar P_5^- anion in the P_5M ($M=Li, Na, \text{ and } K$) clusters. *J. Mol. Struct.* **713**, 113–117 (2005).
34. Gross, L. et al. Bond-order discrimination by atomic force microscopy. *Science* **337**, 1326–1329 (2012).
35. Zhong, Q. et al. On-surface synthesis and real-space visualization of aromatic P_3N_3 . *Angew. Chem. Int. Ed.* **62**, e202310121 (2023).
36. Boneschanscher, M. P., Hämäläinen, S. K., Liljeroth, P. & Swart, I. Sample corrugation affects the apparent bond lengths in atomic force microscopy. *ACS Nano* **8**, 3006–3014 (2014).
37. Kawai, S. et al. Diacetylene linked anthracene oligomers synthesized by one-shot homocoupling of trimethylsilyl on Cu(111). *ACS Nano* **12**, 8791–8797 (2018).
38. Gonzalez-Lakunza, N. et al. Formation of dispersive hybrid bands at an organic-metal interface. *Phys. Rev. Lett.* **100**, 156805 (2008).
39. Nony, L., Foster, A. S., Bocquet, F. & Loppacher, C. Understanding the atomic-scale contrast in Kelvin probe force microscopy. *Phys. Rev. Lett.* **103**, 036802 (2009).
40. Sadeghi, A. et al. Multiscale approach for simulations of Kelvin probe force microscopy with atomic resolution. *Phys. Rev. B* **86**, 075407 (2012).
41. Bädler, M. & Ouzounis, D. Beiträge zur chemie des phosphors, 194 [1] natriumpentaphosphacyclopentadienid: darstellung aus weissem phosphor und natriumdihydrogenphosphid. *Z. Naturforsch. B* **44**, 381–382 (1989).
42. Scherer, O. J., Schwalb, J., Wolmershäuser, G., Kaim, W. & Gross, R. cyclo-P5 as Complex ligand—the phosphorus analogue of the cyclopentadienyl ligand. *Angew. Chem. Int. Ed.* **25**, 363–364 (1986).
43. Li, C. et al. Strong signature of electron-vibration coupling in molecules on Ag(111) triggered by tip-gated discharging. *Nat. Commun.* **14**, 5956 (2023).
44. Hofmann, O. T. et al. Orientation-dependent work-function modification using substituted pyrene-based acceptors. *J. Phys. Chem. C* **121**, 24657–24668 (2017).
45. Giessibl, F. J. The qPlus sensor, a powerful core for the atomic force microscope. *Rev. Sci. Instrum.* **90**, 011101 (2019).
46. Pawlak, R., Kawai, S., Fremy, S., Glatzel, T. & Meyer, E. Atomic-scale mechanical properties of orientated C_{60} molecules revealed by noncontact atomic force microscopy. *ACS Nano* **5**, 6349–6354 (2011).
47. Bartels, L. et al. Dynamics of electron-induced manipulation of individual CO molecules on Cu (111). *Phys. Rev. Lett.* **80**, 2004 (1998).
48. Hapala, P. et al. Mechanism of high-resolution STM/AFM imaging with functionalized tips. *Phys. Rev. B* **90**, 085421 (2014).
49. Kresse, G. & Furthmüller, J. Efficient iterative schemes for ab initio total-energy calculations using a plane-wave basis set. *Phys. Rev. B* **54**, 11169–11186 (1996).
50. Perdew, J. P., Burke, K. & Ernzerhof, M. Generalized gradient approximation made simple. *Phys. Rev. Lett.* **77**, 3865–3868 (1996).
51. Grimme, S., Antony, J., Ehrlich, S. & Krieg, H. A consistent and accurate ab initio parametrization of density functional dispersion correction (DFT-D) for the 94 elements H-Pu. *J. Chem. Phys.* **132**, 154104 (2010).
52. Pawlak, R. Probing charge redistribution at the interface of self-assembled cyclo-P5 pentamers on Ag(111) [Data set]. *Zenodo* <https://doi.org/10.5281/zenodo.110914> (2024).

Acknowledgements

E.M. and R.P. acknowledge funding from the Swiss Nanoscience Institute (SNI), the European Research Council (ERC) under the European Union's Horizon 2020 research and innovation program (ULTRADISS grant agreement No 834402 and support as a part of NCCR SPIN, a National Center of Competence (or Excellence) in Research, funded by the SNF (grant number 51NF40-180604). E.M. and T.G. acknowledge the Sinergia Project funded by the SNF (CRSII5_213533). E.M., T.G., and R.P. acknowledge the SNF grant (200021_228403). T.G. acknowledges the FET-Open program (Q-AFM grant agreement No 828966) of the European Commission. J.-C.L. acknowledges funding from the European Union's Horizon 2020 research and innovation program under the Marie Skłodowska-Curie grant agreement number 847471. C.L. and E.M. acknowledge the Georg H. Endress Foundation.

Author contributions

R.P. and E.M. conceived the experiments. O.C. and R.P. performed the STM/AFM measurements with support from J.-C.L. and C.L. Y.Y., F.D., and Q.Y. performed DFT calculations. O.C. and R.P. analyzed the data. R.P. wrote the manuscript. O.C., Y.Y., J.-C.L., C.L., T.G., F.D., Q.Y., E.M., and R.P. discussed the results and revised the manuscript.

Competing interests

The authors declare no competing interests.

Additional information

Supplementary information The online version contains supplementary material available at <https://doi.org/10.1038/s41467-024-50862-4>.

Correspondence and requests for materials should be addressed to Ernst Meyer or Rémy Pawlak.

Peer review information *Nature Communications* thanks Daniel Ebelin and the other anonymous, reviewer(s) for their contribution to the peer review of this work. A peer review file is available.

Reprints and permissions information is available at <http://www.nature.com/reprints>

Publisher's note Springer Nature remains neutral with regard to jurisdictional claims in published maps and institutional affiliations.

Open Access This article is licensed under a Creative Commons Attribution-NonCommercial-NoDerivatives 4.0 International License, which permits any non-commercial use, sharing, distribution and reproduction in any medium or format, as long as you give appropriate credit to the original author(s) and the source, provide a link to the Creative Commons licence, and indicate if you modified the licensed material. You do not have permission under this licence to share adapted material derived from this article or parts of it. The images or other third party material in this article are included in the article's Creative Commons licence, unless indicated otherwise in a credit line to the material. If material is not included in the article's Creative Commons licence and your intended use is not permitted by statutory regulation or exceeds the permitted use, you will need to obtain permission directly from the copyright holder. To view a copy of this licence, visit <http://creativecommons.org/licenses/by-nc-nd/4.0/>.

© The Author(s) 2024